Materials Research Bulletin 129 (2020) 110903

Contents lists available at ScienceDirect

Materials Research Bulletin

journal homepage: www.elsevier.com/locate/matresbu

Boosted photocatalytic elimination toward Cr(VI) and organic pollutants over BUC-21/$Cd_{0.5}Zn_{0.5}S$ under LED visible Light

Xian Wei, Peng Wang, Huifen Fu, Chen Zhao, Chong-Chen Wang*

Beijing Key Laboratory of Functional Materials for Building Structure and Environment Remediation, School of Environment and Energy Engineering, Beijing University of Civil Engineering and Architecture, Beijing 100044, China

ARTICLE INFO

Keywords:
BUC-21
$Cd_{0.5}Zn_{0.5}S$
Cr(VI) sequestration
organic pollutant decomposition
photocatalysis

ABSTRACT

Series BUC-21/$Cd_{0.5}Zn_{0.5}S$ (B100C*X*, *X* = 20, 60, 100) were prepared by simply ball-milling the mixture of BUC-21 and $Cd_{0.5}Zn_{0.5}S$ at 30 HZ for 20 min. The photocatalytic activities of B100C*X* under the illuminance of low power LED visible light were estimated. According to influencing factor experiments, it was revealed that B100C*X* composites displayed better Cr(VI) sequestration performances than pristine BUC-21 and individual $Cd_{0.5}Zn_{0.5}S$, resulting from the effective separation of photo-induced electron-hole pairs and the inhibited aggregation of the $Cd_{0.5}Zn_{0.5}S$ nano-particles. The photoluminescence, electrochemical analysis, active species trapping experiments and electron spin resonance (ESR) provided further evidence for improved photocatalytic activity. After three cycles, the photocatalytic Cr(VI) sequestration efficiency over B100C100 was still more than 90%, implying that B100C100 displayed remarkable recyclability and stability. At last, the corresponding photocatalytic mechanism over B100C*X* was proposed and verified by some techniques.

1. Introduction

Recently, water shortage resulted from natural disasters, population increase and water pollution becomes a serious problem faced by the current world, and providing sustainable solutions to control pollution is a huge challenge [1]. Typically, pollutants in water include but not limited to organic pollutants like organic dyes and pharmaceutical and personal care products (PPCPs) [2,3] as well as heavy metal ions like Cr (VI) [4]. Among various heavy metal ions and organic contaminants, Cr (VI) and some organic dyes are simultaneously existed in water environment due to their chemical stability. Converting Cr(VI) into Cr(III) is an common method to manage chromium pollution, considering that the level of danger of Cr(III) are relatively weak [5]. Chemical-, biological- and electro- sequestration methods are usually used to accomplish Cr(VI) reduction into Cr(III) [6]. Especially, $Cr(OH)_3$ precipitate formed at neutral or alkaline conditions can be easily removed from water [7]. Generally, the organic dyes are cleaned by adsorption [8], membrane [9] and biodegradation [10,11]. However, all the above solutions are limited due to high operation costs, strict working conditions and potential formation of secondary pollutants. Photocatalysis have gradually developed over the past decades with the merits like low cost, high efficiency and potential utilization of sunlight [12–14].

The visible light responsive photocatalyst $Cd_xZn_{1-x}S$ possesses a adjustable composition and band gap [15,16]. The formation of $Cd_xZn_{1-x}S$ is considered as a feasible way to overcome the disadvantages of pristine CdS and ZnS [17–19]. Especially, by changing the proportion of CdS and ZnS, the band edge position and the band gap width of $Cd_xZn_{1-x}S$ can be flexibly tuned [15]. The $Cd_xZn_{1-x}S$ solid solution displayed effectively photocatalytic activity in producing H_2 from water splitting and organic pollutants degradation upon the illumination of visible light [20–23]. However, the individual $Cd_xZn_{1-x}S$ still suffered from the disadvantages like less active sites [22], poor electron-hole separation efficiency [24] and weak photo-excited charge carriers mobility [20]. Some methods like doping with noble metals [21], combination with semiconductors photocatalysts [24,25] have been carried out to accomplish boosted photocatalytic ability of $Cd_xZn_{1-x}S$.

Recently, porous coordination polymers (PCPs) as well as metal organic frameworks (MOFs) and their composites have attracted more interests from many fields like chemical sensing [26], gas storage and separation [27], drug delivery [28], photoelectrochemistry [29] and photocatalysis [30–33] resulting from their tunable structures [34] and high specific surface areas [35]. Wang and coworkers proposed that the MOFs or CPs with huge surface area can provide an ideal platform to distribute nanoparticles or nanosheets uniformly and/or act as co-photocatalyst, which can further improve the light absorption behavior [36,37]. Up to now, some $Cd_xZn_{1-x}S$@MOFs have been reported, in which only the obtained $Cd_{0.5}Zn_{0.5}S$@ZIF-8 was used as photocatalyst

* Corresponding author.
E-mail addresses: wangchongchen@bucea.edu.cn, chongchenwang@126.com (C.-C. Wang).

https://doi.org/10.1016/j.materresbull.2020.110903
Received 30 January 2020; Received in revised form 19 April 2020; Accepted 19 April 2020
Available online 24 April 2020

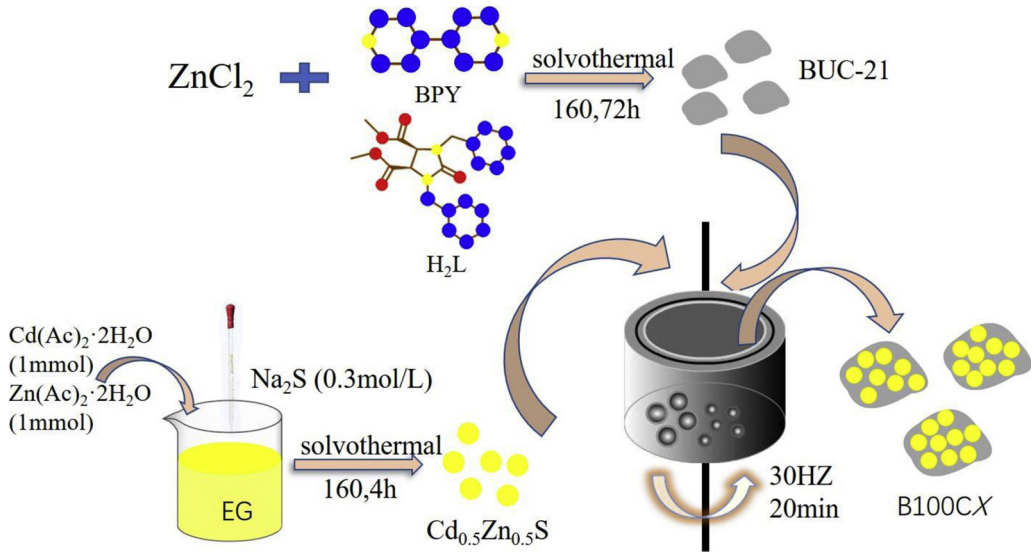

Scheme 1. Illustration of the BUC-21/$Cd_{0.5}Zn_{0.5}S$ (B100C*X*) composites fabrication.

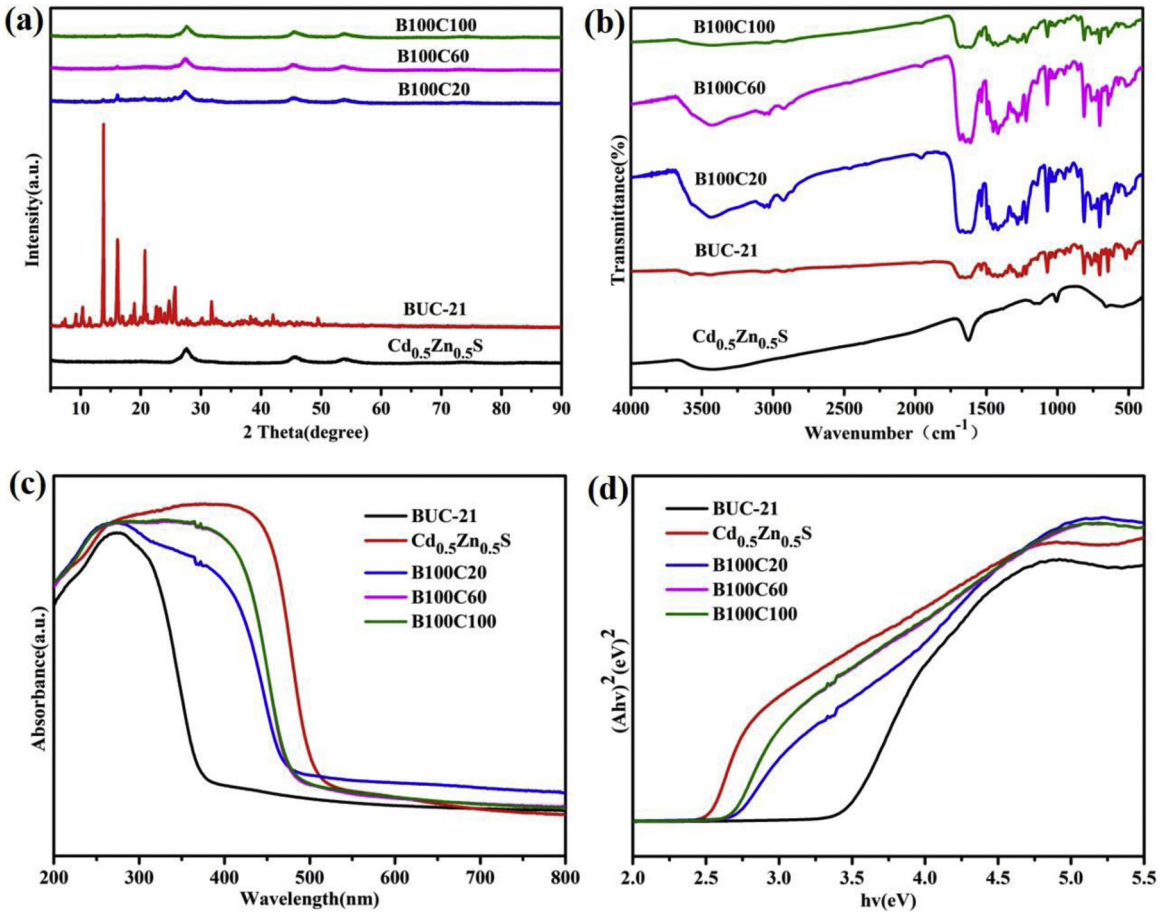

Fig. 1. (a) PXRD patterns, (b) FTIR spectra and (c) UV–vis DRS and (d) E_g plot of BUC-21, $Cd_{0.5}Zn_{0.5}S$ and the series of composites.

to achieve Cr(VI) sequestration [38–40].

BUC-21, known as a 2D coordination polymer Zn(bpy)L (bpy = 4,4'-bipyridine; L = *cis*-1,3-dibenzyl-2-imidazolidone-4,5-dicarboxylic acid), was firstly reported by our research group, which exhibited outstanding photocatalytic performances toward Cr(VI) reduction and organic dyes degradation under UV light illumination [41]. To broaden the responsive light length to visible region, the g-C_3N_4, $Bi_{24}O_{31}Br_{10}$ nanosheets and N-$K_2Ti_4O_9$ were introduced to fabricate the BUC-21/g-C_3N_4, BUC-21/$Bi_{24}O_{31}Br_{10}$ and BUC-21/N-$K_2Ti_4O_9$ composites used as effective Cr(VI) sequestration under visible light [42–44]. The hollow titanate nanotubes (TNTs) with ultrahigh adsorption capacity toward cationic heavy metal ions were adopted to prepare BUC-21/TNTs, which can achieve simultaneously photocatalytic and adsorptive removal of Cr(VI) ions and the formed Cr(III) [45].

Within this work, BUC-21 was selected to act as platform to distribute the $Cd_{0.5}Zn_{0.5}S$ nanoparticles uniformly for constructing BUC-

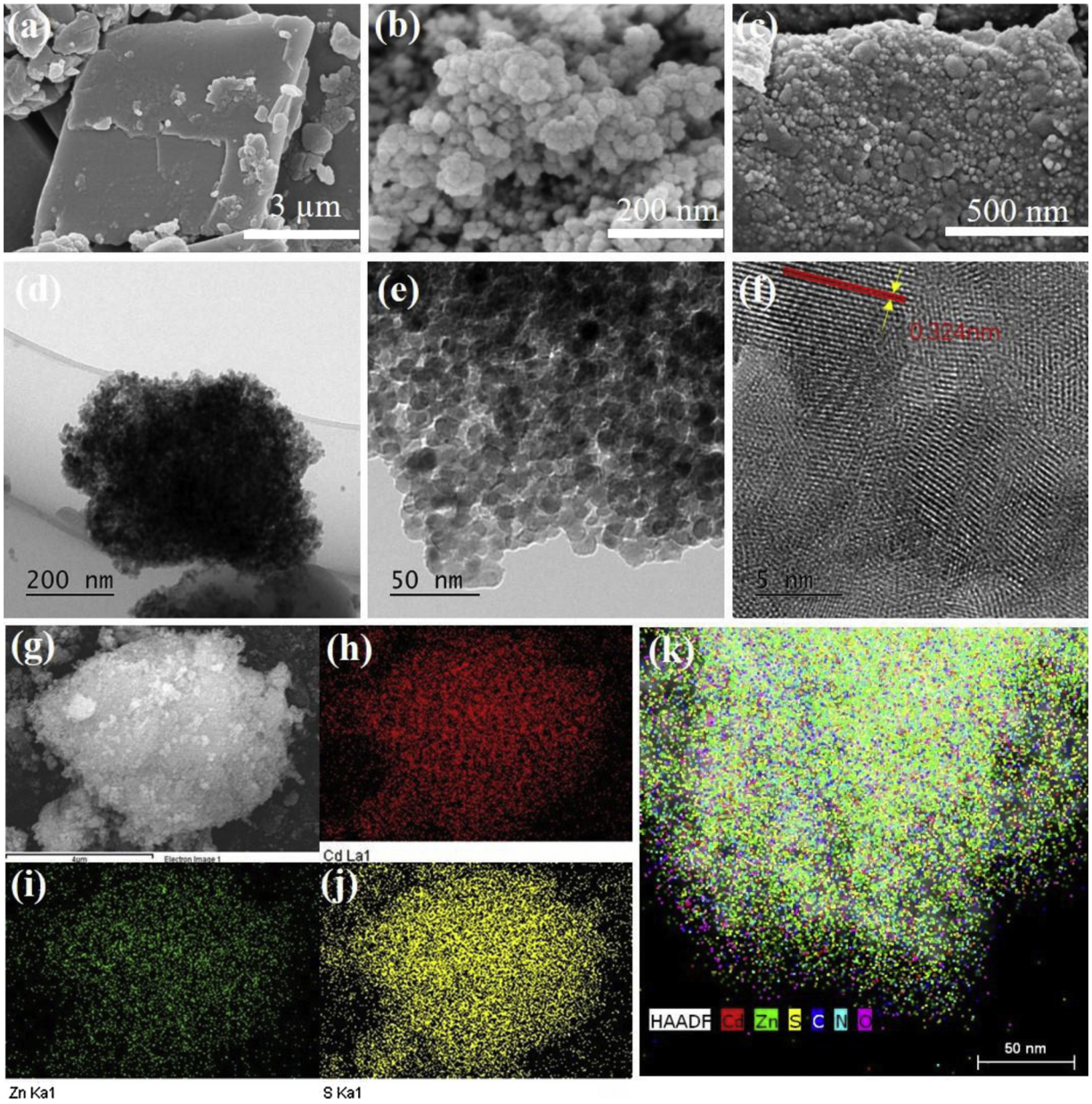

Fig. 2. SEM images of (a) BUC-21, (b) $Cd_{0.5}Zn_{0.5}S$ and (c) B100C100. (d, e) TEM images and (f) HRTEM image of B100C100. (g, h, i, j) EDX elemental mapping of $Cd_{0.5}Zn_{0.5}S$ and (k) HAADF image of B100C100.

21/$Cd_{0.5}Zn_{0.5}S$ composites, which can accomplish boosted photocatalytic performance towards Cr(VI) sequestration and organic dyes decomposition under visible light. Finally, the photocatalytic influencing factors and corresponding mechanism were investigated.

2. Experimental

2.1. Materials and characterization

All consumables are commercially available, which were used directly without further treatments. As well, the characterization methods, the photocatalytic activity experiments and recyclability tests experiments are given in the Supporting Information. Most worthy of mention is that the photocatalytic performances of B100C*X* composites were assessed under low-power visible (a 5.00 W LED light source, PCX50C, Beijing Perfect Light Technology Co., Ltd.), and the spectrum of light source was shown in Fig. S1. The residual Cr(VI) was determined by diphenylcarbazide (DPC) method via Auto Analyzer 3 (Seal, Germany) (The image of Auto Analyzer 3 are shown in Fig. S2).

2.2. Preparation of BUC-21/$Cd_{0.5}Zn_{0.5}S$ composites

The BUC-21 was hydrothermally synthesized following a previous report [41] and the $Cd_{0.5}Zn_{0.5}S$ were synthesized according to previous report [40], which were described detailly in the Supporting Information.

The BUC-21/$Cd_{0.5}Zn_{0.5}S$ composites were fabricated by ball-milling the as-prepared BUC-21 and $Cd_{0.5}Zn_{0.5}S$ at 30 Hz for 20 min (Scheme 1). Series BUC-21/$Cd_{0.5}Zn_{0.5}S$ composites were named as B100C20 (100 mg BUC-21, 20 mg $Cd_{0.5}Zn_{0.5}S$), B100C60 (100 mg BUC-21, 60 mg $Cd_{0.5}Zn_{0.5}S$) and B100C100 (100 mg BUC-21, 100 mg $Cd_{0.5}Zn_{0.5}S$), respectively.

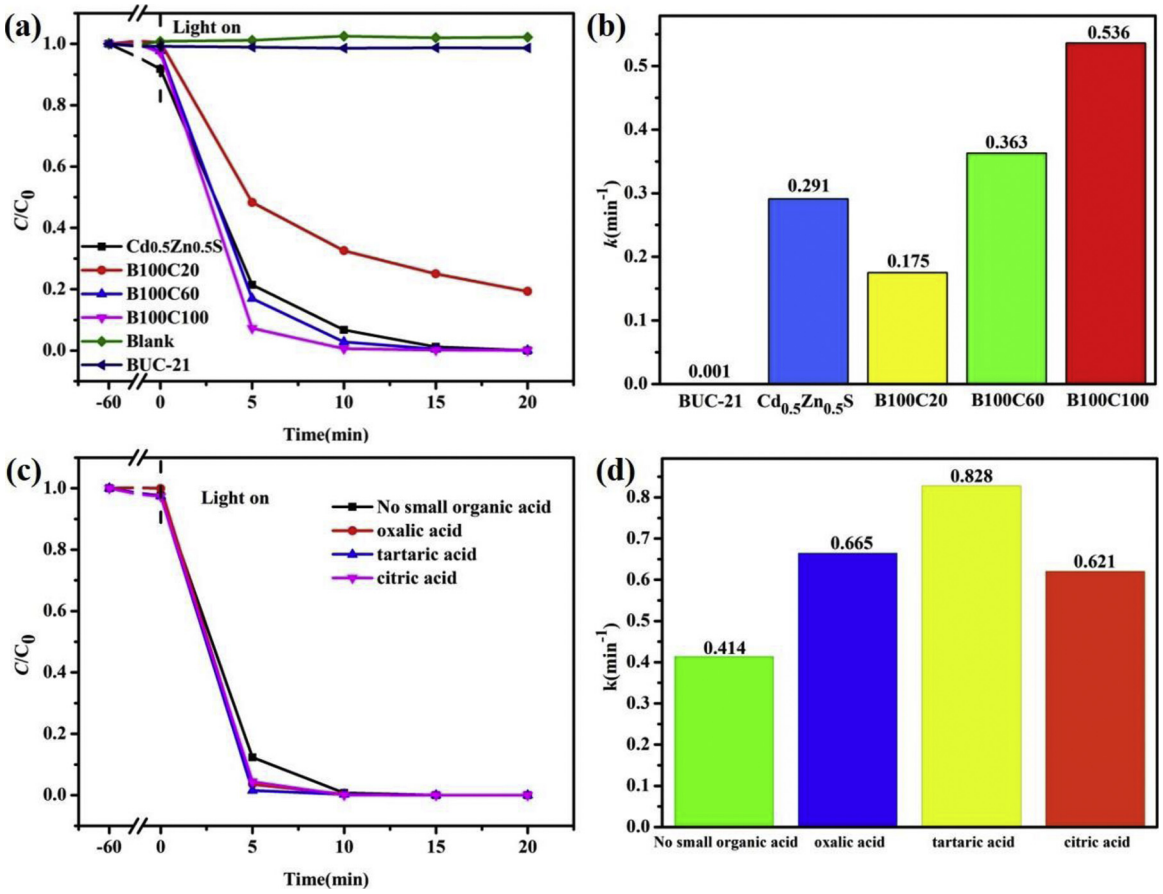

Fig. 3. (a) Photocatalytic sequestration of Cr(VI) and (b) The photocatalytic sequestration rates (k values) over the as-prepared $Cd_{0.5}Zn_{0.5}S$ (10 mg), BUC-21 and B100C*X* composites under visible-light irradiation; Effects of different small organic compounds on the (c) Cr(VI) sequestration and (d) photocatalytic Cr(VI) sequestration rates (k values). Conditions: Cr(VI) = 10 mg/L, volume: 50 mL, pH = 5.0, small organic acid dosage: 0.5 mmol/L. photocatalyst dosage: 400 mg/L.

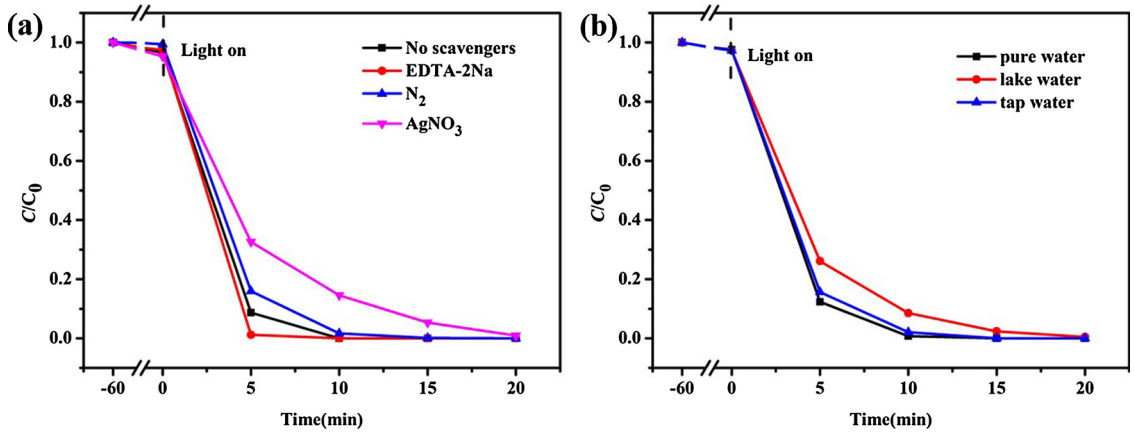

Fig. 4. The effects of (a) different scavengers and (b) foreign ions on the sequestration of Cr(VI) in the presence of B100C100 under visible light irradiation. Conditions: B100C100 = 400 mg/L, Cr(VI) = 10 mg/L, 50 mL, pH = 5.0, scavengers dosage: 0.5 mmol/L.

3. Results and discussion

3.1. Characterization

The powder XRD patterns of the different materials are demonstrated in Fig. 1a, in which the XRD patterns of $Cd_{0.5}Zn_{0.5}S$ and BUC-21 were the same as those reported in the literature [41,46]. The characteristic diff ;raction peaks at 2θ being 27.4°, 45.5° and 53.8° of $Cd_{0.5}Zn_{0.5}S$ correspond to the (111), (220) and (311) planes of cubic zinc-blende structure phase [47]. The peaks at 13.8° and 16.1° of all B100C*X* composites belong to the characteristic peaks of pure BUC-21. However, the peak intensities of BUC-21 decrease with the increasing $Cd_{0.5}Zn_{0.5}S$ contents in B100C60 and B100C100.

The FTIR spectra displayed in Fig. 1b proved the successful fabrication of B100C*X* composites. The peak at 1648 and 1420 cm^{-1} corresponded to the asymmetric and symmetric vibrations of COO- groups, respectively. The peak at 1220 cm^{-1} was assigned to the ν (C-N) of the phenyl rings in BUC-21, which was in consist with the counterpart report [45].

As shown in Fig. 1c and d, the original BUC-21 demonstrated no

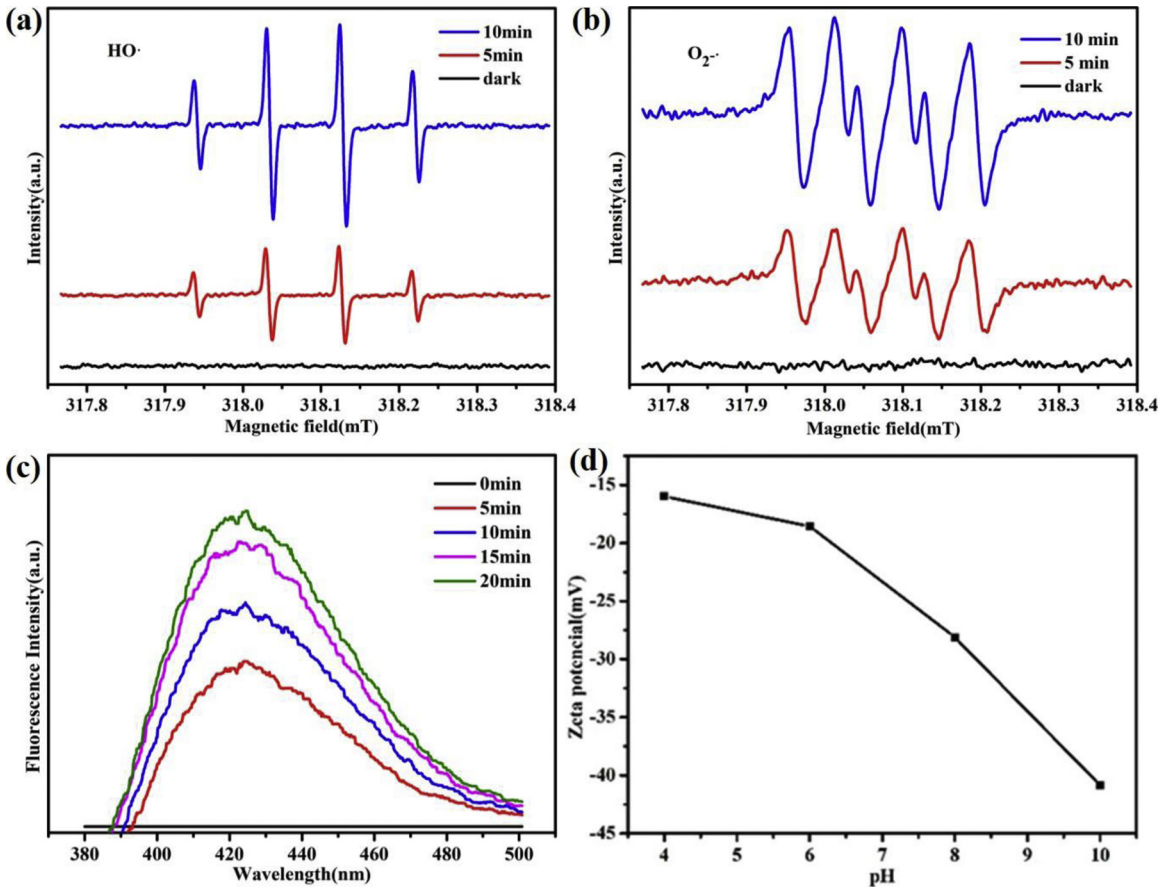

Fig. 5. ESR spectra of different radicals trapped by DMPO for •OH (a) and $•O_2^-$ (b) over B100C100, (c) Fluorescence spectral changes of different irradiation time (excitation at 315 nm) observed over B100C100 upon the irradiation of visible light. (d) Zeta potentials of B100C100 under different pH. Experimental conditions: B100C100 = 400 mg/L; terephthalic acid, 0.5 mM; NaOH, 2 mM.

visible light absorption ability. The absorption edge of pristine $Cd_{0.5}Zn_{0.5}S$ appears at 470 nm with the band-gap value being 2.53 eV. The addition of $Cd_{0.5}Zn_{0.5}S$ into BUC-21 could transfer the absorption region from UV light (E_g = 3.49 eV) to visible light (E_g = 2.68 eV) for B100C*X* composites, indicating that the B100C*X* composites could show photocatalytic abilities under visible light [48]. The band gap values of the composites are located between the values of the two components due to the composites combine the optical properties of both $Cd_{0.5}Zn_{0.5}S$ and BUC-21, which is consistent with the situation reported in the literatures [49,50].

The successful fabrication of BUC-21/$Cd_{0.5}Zn_{0.5}S$ was further proved using SEM, TEM and HRTEM. The SEM image indicated that the individual BUC-21 particles present an irregular bulk structure (Fig. 2a). $Cd_{0.5}Zn_{0.5}S$ presents regular small spherical of different size from 20 nm to 40 nm (Fig. 2b). Both SEM and TEM images illustrated that $Cd_{0.5}Zn_{0.5}S$ nanoparticles are adhered to the surface of BUC-21 (Fig. 2c–e). According to the HRTEM image of B100C100 (Fig. 2f), the lattice fringe of 0.324 nm corresponds to the (111) facet of $Cd_{0.5}Zn_{0.5}S$. The elements of Cd, Zn and S are evenly scattered on B100C100 (Fig. 2k), which further indicates that $Cd_{0.5}Zn_{0.5}S$ is successfully loaded on the surface of BUC-21 [40].

3.2. Photocatalytic performances

3.2.1. Photocatalytic Cr(VI) sequestration

The photocatalytic abilities of BUC-21, $Cd_{0.5}Zn_{0.5}S$, B100C20, B100C60 and B100C100 for Cr(VI) sequestration were performed under visible light. Series BUC-21/$Cd_{0.5}Zn_{0.5}S$ composites demonstrated better photocatalytic abilities for Cr(VI) sequestration than those of individual BUC-21 and $Cd_{0.5}Zn_{0.5}S$ under identical conditions (Fig. 3a), in which Cr(VI) was completely deoxidized over B100C100 as photocatalyst without the addition of hole consumer within 20 min. It was observed that Cr(VI) sequestration activities were significantly boosted following the order of B100C100 > B100C60 > B100C20 > $Cd_{0.5}Zn_{0.5}S$ > BUC-21. It was described by pseudo-first-order kinetics (Equation (S1) as listed in ESI) to further study and understand the kinetics of Cr(VI) sequestration over different photocatalysts. As shown in Fig. 3b, after 5 min of lighting, the photocatalytic rates followed the order of B100C100 > B100C60 > $Cd_{0.5}Zn_{0.5}S$ > B100C20 > BUC-21.

3.2.1.1. Influences of different organic acids. The consumption of hole (h^+) will improve the separation of the photoinduced charge carriers to achieve enhanced Cr(VI) sequestration efficiency. Small organic acids are often used as hole scavengers on the Cr(VI) sequestration, like citric acid, tartaric acid and oxalic acid. In Fig. 3c, the addition of small organic acids can enhance the photocatalytic sequestration efficiency of Cr(VI) over B100C100 under visible light.

In Fig. 3d, the *k* values following the order of tartaric acid (0.828 min^{-1}) > oxalic acid (0.665 min^{-1}) > citric acid (0.621 min^{-1}) > no hole scavenger (0.414 min^{-1}). The increase of reaction rate may result from the number of α–hydroxyl carboxylate groups. The tartaric acid has more α–hydroxyl groups compared with oxalic acid and citric acid [42].

3.2.1.2. Influences of foreign ions. The foreign ions including inorganic ions and organic matter have a certain effect on the photocatalytic Cr (VI) sequestration activity. In the experiment, the real lake water and real tap water (collected in Daxing campus of BUCEA) were used to

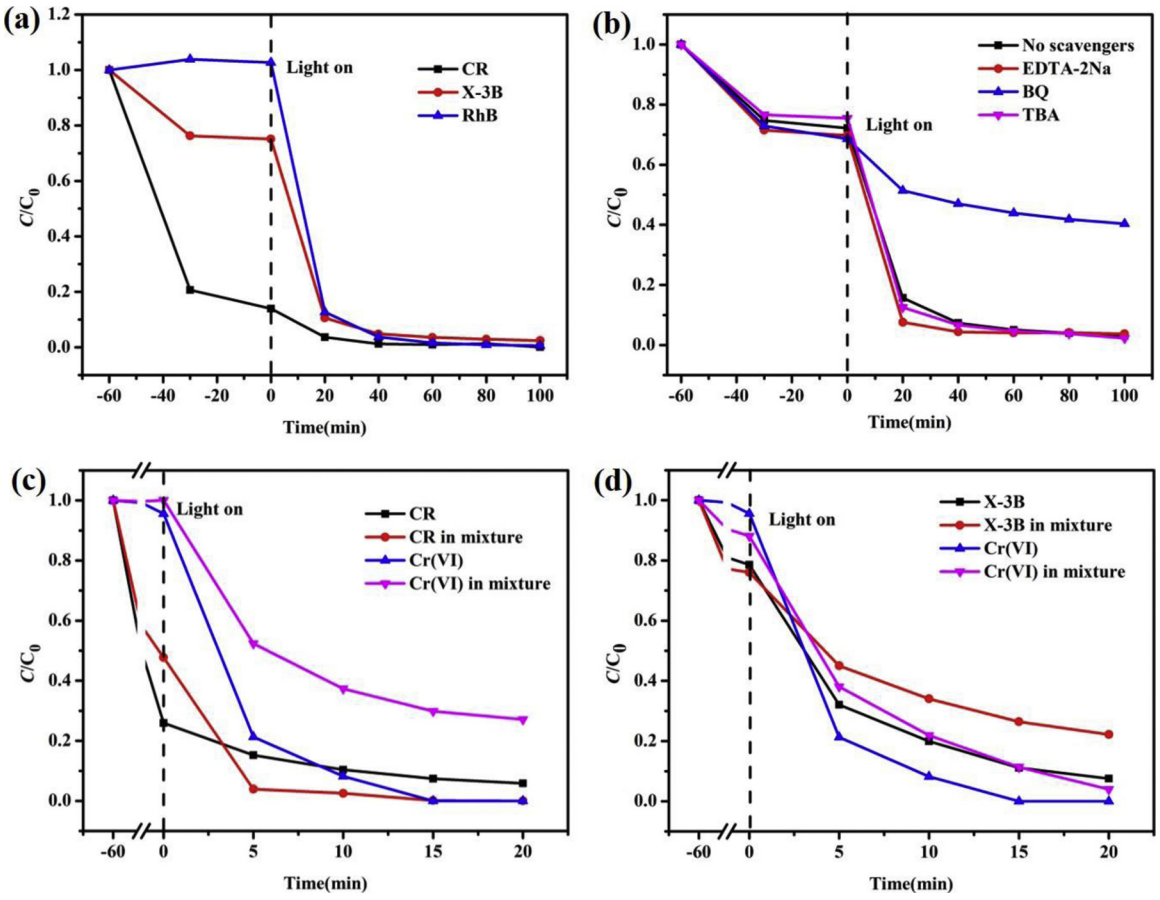

Fig. 6. (a) The photocatalytic degradation of B100C100 towards different organic dyes (RhB, CR, X-3B). (b) Eff ;ects of different scavengers on the degradation of X-3B over B100C100 under visible light irradiation. Photocatalytic Cr(VI) sequestration and (c) CR, (d) X-3B degradation efficiencies in single and mixed systems with B100C100 as photocatalyst. Reaction conditions: (a) 20 mg B100C100, 50 mL of RhB (10 mg/L) or X-3B (50 mg/ L) or CR (50 mg/L). (b) 20 mg B100C100, 50 mL of X-3B (50 mg/L). (c) 20 mg B100C100, 50 mL of CR (50 mg/L) and Cr(VI) (10 mg/L). (d) 20 mg B100C100, 50 mL of X-3B (50 mg/L) and Cr(VI) (10 mg/L).

prepare Cr(VI) solution, respectively. As shown in Fig. 4b, no significant decrease in the sequestration of Cr(VI) after the presence of foreign ions under visible light irradiation. The Cr(VI) sequestration efficiencies toward the solutions simulated from tap water and lake water were still close to 100% within 20 min, implying that the foreign ions had little effect on the sequestration of Cr(VI).

3.2.1.3. The exploration of active species towards the Cr(VI) sequestration. To investigate the primary reactive species in the photocatalytic sequestration of Cr(VI), some different scavengers were used to identify the active species and their roles in the photocatalytic processes. Generally, EDTA–2Na (0.5 mmol/L), $AgNO_3$ (0.5 mmol/L) and isopropyl alcohol (IPA, 0.5 mmol/L) were added to the solution to quench h^+, e^- and •HO, respectively. As well, nitrogen gas was pumped into the solution to drive away dissolved oxygen gas (DO) in Cr(VI) solution to suppress the formation of $•O_2^-$. It has been pointed out that e^- is important photoactive substance to control the sequestration of Cr (VI) in previous papers. As displayed in Fig. 4a, the sequestration of Cr (VI) by B100C100 was significantly inhibited when there is $AgNO_3$ or N_2, and improved when there is EDTA-2Na or IPA, indicating that both e^- and $•O_2^-$ were responsible for the Cr(VI) sequestration under visible light. The existence of $•O_2^-$ and •HO could be further affirmed by the electron spin resonance (ESR) determination, as shown in Fig. 5a and b. Especially, the concentration of •HO was further confirmed by fluorescence intensity. Fluorescence peak changes (excitation at 315 nm) were shown in Fig. 5c. With the irradiation time increases, the fluorescence intensity at 425 nm improves obviously.

3.2.2. Photo-catalytically oxidative degradation performances

The photocatalytic degradation experiments of B100C100 were conducted with the several organic dyes like rhodamine B (RhB), congo red (CR) and reactive Red (X-3B). As shown in Fig. 6a, during dark adsorption, B100C100 possessed different adsorption performances toward cationic RhB, anionic X-3B and CR. Compared with cationic RhB, B100C100 exhibits better adsorption ability toward anionic X-3B and CR. According to the Zeta potential of B100C100 under different pH values (Fig. 5d), the adsorption performances toward X-3B and CR did not depend on electrostatic effects but possibly hydrogen-bonding interactions and π-π stacking interaction between the ligands in BUC-21 and the organic dyes. However, CR has the proper molecular structure compared with X-3B, which leads to the better adsorption ability toward CR than that toward X-3B. B100C100 displays high adsorption activity toward CR with the adsorption efficiency of 86% within 1 h. Under the visible light irradiation, the degradation efficiencies toward CR and RhB are both close to 100% within 100 min, and ca. 98% X-3B can be degraded. In order to distinguish the surface adsorption and surface degradation of selected organic dyes over B100C100 under dark condition, series experiments were designed, in which the CR solutions with initial concentration of 50 mg/L were selected to carry out adsorption and photocatalytic degradation for 160 min, respectively. After adsorptive treatment, the color of the treated CR solution with lower concentration maintained the color of original CR solution (Fig. S3(a) and (b)). However, after photocatalytic treatment, the yellow color of the solution was different from the red color of original CR solution (Fig. S3(a) and (c)). As well, it can be further affirmed by the colors of the B100C100 after adsorption and after photocatalysis. After

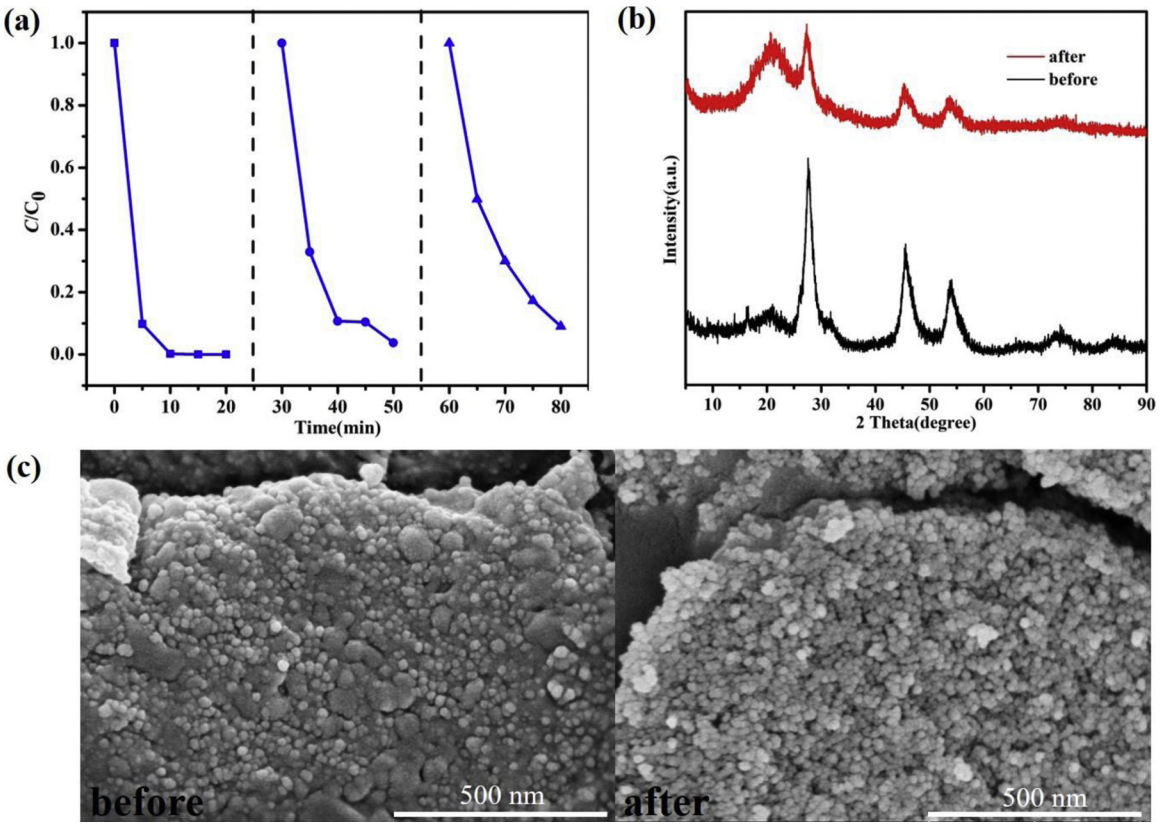

Fig. 7. (a) cycling runs for the photocatalytic Cr(VI) sequestration in the presence of B100C100 under visible light irradiation. (b) The PXRD and (c) SEM image of B100C100 before and after three cycles.

adsorption, the originally yellow color of B100C100 changed into red (the color of CR), implying that CR was physically adsorbed onto B100C100 (Fig. S4(a) and (b)). After photocatalysis, the B100C100 maintained as yellow color identical to the original B100C100 (Fig. S4(a) and (c)). It can be concluded that under dark condition, CR was adsorbed onto B100C100, while, CR was degraded into other forms different from CR upon the irradiation of light. In all, B100C100 demonstrated excellent photocatalytic degradation performance towards different organic dyes [51].

3.2.2.1. The identification of active species during the organic dyes degradation. It was essential to identify the active species during the photocatalysis reaction over photocatalysts toward different organic pollutants. In this work, the active species trapping tests were carried out via adding different scavengers (EDTA-2Na, BQ and TBA). The concentration of all three is 0.5 mmol/L. It was well known that •HO and $\bullet O_2^-$ are important active radicals to degrade organic pollutants in previous papers [52,53]. As depicted in Fig. 6b, the degradation of X-3B over B100C100 was obviously inhibited after the addition of benzoquinone (BQ, 0.5 mmol/L), indicating that $\bullet O_2^-$ as the main active specie can achieve oxidative degradation of organic dyes under visible light.

3.2.3. The photocatalytic activity in the mixed system

As all known, the composition of pollutants in industrial wastewater is complex. Heavy metals such as Cr(VI) are commonly existed in industrial wastewater with different organic pollutants. In this paper, B100C100 was used as photocatalyst to accomplish Cr(VI) sequestration and organic dyes degradation simultaneously. As depicted in Fig. 6c and d, in the single system of Cr(VI) and X-3B/CR, B100C100 could achieve 100% Cr(VI) sequestration, 94% CR and 92% X-3B degradation after 20 min' illumination, respectively. While, for the Cr(VI) and CR matrix, 100% CR was removed in 20 min, possibly due to the more exposed active sites resulting from the less adsorption towards CR and the quick capture of Cr(VI) towards electrons. In the Cr(VI) and X-3B mixture system, the removal efficiency towards both Cr(VI) and X-3B by B100C100 became lower than the single system, possibly due to the race between Cr(VI) and X-3B towards $\bullet O_2^-$.

3.2.4. Reusability and stability of B100C100

For practical application of B100C100, the reusability and stability must be considered. As depicted in Fig. 7a, the photocatalytic Cr(VI) sequestration efficiency of B100C100 was more than 90% after three cycles. As well, as shown in Fig. 7b, the major XRD peaks remained, but the crystallinity of the catalyst was lower than that before photocatalysis, indicating that the structure of the composites was slightly affected. It was possibly assigned to that the crystallinity of BUC-21 decreased after soaking in the solution for a period of time [54]. However, no noticeable changes were occurred in the morphologies of B100C100. It was possibly attributed to that $Cd_{0.5}Zn_{0.5}S$ nanoparticles were partially detached from the appearance of the BUC-21 [55], which could be observed from the SEM images, implying that B100C100 possesses good reusability and stability.

3.2.5. Photocatalytic reaction mechanism

To understand the photocatalysis mechanism over BUC-21/$Cd_{0.5}Zn_{0.5}S$ composites, the separation efficiency of carrier charges was tested by photoluminescence (PL). Fig. 8a presents the PL spectra of the pure $Cd_{0.5}Zn_{0.5}S$, B100C20, B100C60 and B100C100 samples excited by the light 360 nm. The pure $Cd_{0.5}Zn_{0.5}S$ exhibits an outstanding emission peak at 418 nm. With the addition of BUC-21, the PL emission intensity decrease obviously, suggesting that the photoinduced charge could be efficiently separated when the $Cd_{0.5}Zn_{0.5}S$ was evenly distributed on BUC-21 producing an interface.

The EIS measurements were conducted to further investigate the interface charge motion of B100C100, BUC-21 and $Cd_{0.5}Zn_{0.5}S$ samples.

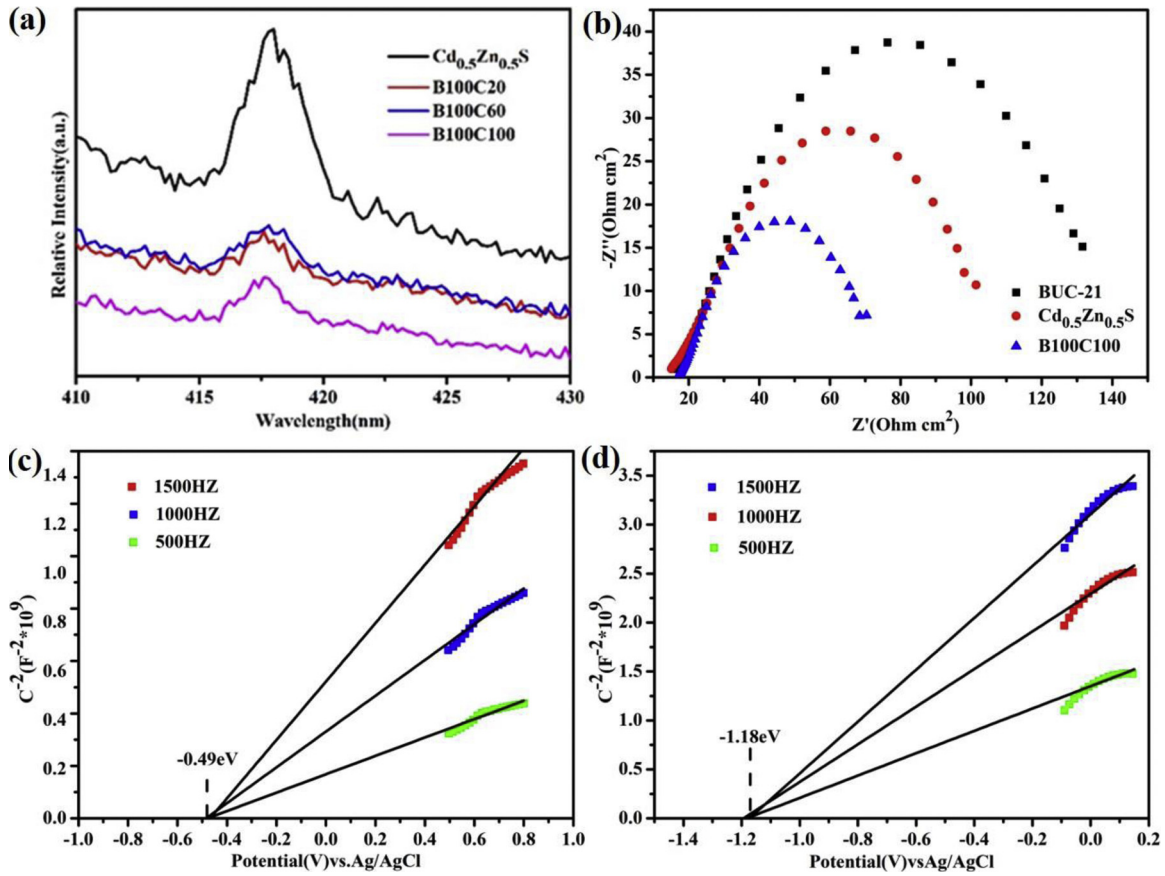

Fig. 8. (a) PL spectra of series B100C*X* composites. (b) Electrochemical impedance spectra (EIS) of BUC-21, $Cd_{0.5}Zn_{0.5}S$ and B100C100. The Mott–Schottky curves of (c) $Cd_{0.5}Zn_{0.5}S$ and (d) BUC-21 at various frequencies.

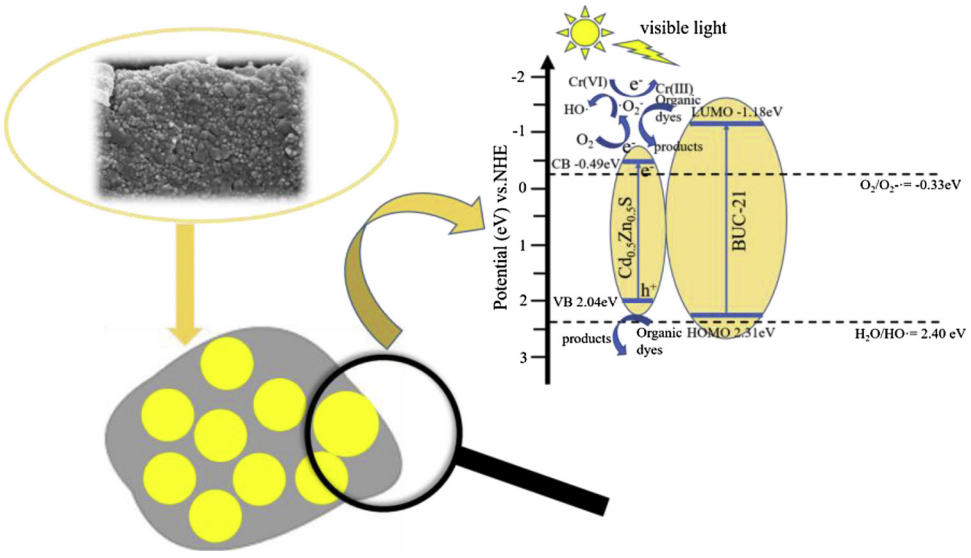

Scheme 2. The proposed mechanism over B100C100 as photocatalyst under visible light.

As shown in Fig. 8b, the smaller arc radius of B100C100 than those of pristine BUC-21 and $Cd_{0.5}Zn_{0.5}S$ implies that a more rapid interfacial transportation and more efficient separation of photo-induced electrons and holes over the composite B100C100.

As depicted in Fig. 8c and d, the Mott-Schottky plots show that the flat band potentials of BUC-21 and $Cd_{0.5}Zn_{0.5}S$ are observed to be approximately -1.18 eV and -0.49 eV versus AgCl/Ag at pH being 5.0, respectively. Considering the band gap value (E_g(BUC-21) = 3.49 eV, E_g ($Cd_{0.5}Zn_{0.5}S$) = 2.53 eV) and E_{FB} in Mott–Schottky, the HOMO of BUC-21 and VB of $Cd_{0.5}Zn_{0.5}S$ were 2.31 eV and 2.04 eV at pH = 5.0, respectively.

According to the corresponding analyses, a possible photocatalytic mechanism for the removal of Cr(VI) and organic dyes under visible light were proposed (Scheme 2). Upon the irradiation of visible light, the electrons (e^-) in the valence band (VB) of $Cd_{0.5}Zn_{0.5}S$ are quickly excited to the conduction band (CB), leaving the holes (h^+) in the VB,

and due to the intimate interfacial contact between BUC-21 and $Cd_{0.5}Zn_{0.5}S$ under mechanical force, which enhances the photo-induced electrons motion efficiency and improves both the stability and uniform distribution of $Cd_{0.5}Zn_{0.5}S$ nanoparticles. The EIS results showed that B100C100 possessed a lower charge-transfer resistance than that of the pristine $Cd_{0.5}Zn_{0.5}S$. It was deemed that BUC-21 a platform can prevent the agglomeration of $Cd_{0.5}Zn_{0.5}S$ nanoparticles to expose more active sites and to achieve the boosted photocatalytic activity [56]. The $\bullet O_2^-$ is a key active substance to accomplish both the direct sequestration of Cr (VI) via Eqs. 3 – 4 and oxidative degradation of organic dyes [57,58]. As the CB value of $Cd_{0.5}Zn_{0.5}S$ is –0.49 eV vs NHE, more negative than the standard redox potential $E(O_2/\bullet O_2^-)$ (–0.33 eV *vs* NHE). The suppression of Cr(VI) sequestration in nitrogen atmosphere and X-3B degradation with the addition of BQ could further affirmed these results, as shown in Fig. 8b. It was worthy to noting that the electrons on the CB of $Cd_{0.5}Zn_{0.5}S$ will directly take part in the Cr(VI) sequestration via Eqs. 1 – 2 due to the initiative of Cr(VI) to trap electrons [59]. As well, the holes on the VB of $Cd_{0.5}Zn_{0.5}S$ and •HO may also play a smaller role in oxidizing organic dyes compared with $\bullet O_2^-$, and the generation of •HO mainly come from $\bullet O_2^-$ generated from the CB of $Cd_{0.5}Zn_{0.5}S$, though the VB of $Cd_{0.5}Zn_{0.5}S$ was less positive than $H_2O/\bullet HO$ [60].

$$Cr_2O_7^{2-} + 14H^+ + 6e^- \rightarrow 2Cr^{3+} + 7H_2O \quad (1)$$

$$CrO_4^{2-} + 4H_2\,O + 3e^- \rightarrow Cr(OH)_3 \downarrow + 5OH^- \quad (2)$$

$$O_2 + e^- \rightarrow \bullet O_2^- \quad (3)$$

$$\bullet O_2^- + Cr(VI) \rightarrow Cr(V) + O_2 \quad (4)$$

4. Conclusions

The B100C*X* composites were successfully obtained by simple ball-milling, which displayed efficient Cr(VI) sequestration and organic dyes elimination. In particular, the B100C100 composite showed a 1.8 times of photocatalytic sequestration rate compared with pristine $Cd_{0.5}Zn_{0.5}S$ under 5 mins' irradiation. The SEM and HRTEM images of B100C100 demonstrated that the $Cd_{0.5}Zn_{0.5}S$ nanoparticles were uniformly scattered on the surface of BUC-21. The PL analysis and electrochemistry measurement proved that the boosted photocatalytic performances were mainly attributed to the enhanced photo-induced electrons motion as well as the improved stability and dispersity of $Cd_{0.5}Zn_{0.5}S$ nanoparticles. According to the investigation of active species and ESR spectra, the $\bullet O_2^-$ worked as a main active substance to convert Cr(VI) into Cr(III) and degrade organic dyes. It was prospective to witness more MOFs (or CPs) and CdZnS being hybridized into composites for boosted photocatalytic performances.

CRediT authorship contribution statement

Xian Wei: Data curation, Investigation, Visualization, Writing - original draft. **Peng Wang:** Resources, Instrumental. **Huifen Fu:** Validation, Software. **Chen Zhao:** Validation, Software. **Chong-Chen Wang:** Conceptualization, Funding acquisition, Supervision, Project administration, Writing - review & editing.

Declaration of Competing Interests

The authors declare that they have no known competing financial interests or personal relationships that could have appeared to influence the work reported in this paper.

Acknowledgements

This work was supported by National Natural Science Foundation of China (51878023, 51578034), Beijing Natural Science Foundation (8202016) and Beijing Talent Project (2019A22).

Appendix A. Supplementary data

Supplementary material related to this article can be found, in the online version, at doi:https://doi.org/10.1016/j.materresbull.2020.110903.

References

[1] H. Dong, G. Zeng, L. Tang, C. Fan, C. Zhang, X. He, Y. He, An overview on limitations of TiO_2-based particles for photocatalytic degradation of organic pollutants and the corresponding countermeasures, Water Research 79 (2015) 128–146.
[2] Q. Huang, Y. Liu, T. Cai, X. Xia, Simultaneous removal of heavy metal ions and organic pollutant by BiOBr/Ti_3C_2 nanocomposite, Journal of Photochemistry and Photobiology A: Chemistry 375 (2019) 201–208.
[3] R. Ma, S. Zhang, T. Wen, P. Gu, L. Li, G. Zhao, F. Niu, Q. Huang, Z. Tang, X. Wang, A critical review on visible-light-response CeO_2-based photocatalysts with enhanced photooxidation of organic pollutants, Catalysis Today 335 (2019) 20–30.
[4] X. Liu, R. Ma, X. Wang, Y. Ma, Y. Yang, L. Zhuang, S. Zhang, R. Jehan, J. Chen, X. Wang, Graphene oxide-based materials for efficient removal of heavy metal ions from aqueous solution: A review, Environmental Pollution 252 (2019) 62–73.
[5] W. Huang, N. Liu, X. Zhang, M. Wu, L. Tang, Metal organic framework g-C_3N_4/MIL-53(Fe) heterojunctions with enhanced photocatalytic activity for Cr(VI) reduction under visible light, Applied Surface Science 425 (2017) 107–116.
[6] K.G. Pavithra, V. Jaikumar, P.S. Kumar, P. SundarRajan, A review on cleaner strategies for chromium industrial wastewater: Present research and future perspective, Journal of Cleaner Production 228 (2019) 580–593.
[7] P. Zhao, H. Zhang, J. Yu, H. Gao, Y. Cao, Y. Zhu, H. Zhao, Conditions for mutual conversion of Cr(III) and Cr(VI) in aluminum chromium slag, Journal of Alloys and Compounds 788 (2019) 506–513.
[8] A. Molla, Y. Li, B. Mandal, S.G. Kang, S.H. Hur, J.S. Chung, Selective adsorption of organic dyes on graphene oxide: theoretical and experimental analysis, Applied Surface Science 464 (2019) 170–177.
[9] T. Luukkonen, A. Heponiemi, H. Runtti, J. Pesonen, J. Yliniemi, U. Lassi, Application of alkali-activated materials for water and wastewater treatment: a review, Reviews in Environmental Science and Bio/Technology 18 (2019) 271–297.
[10] P. Aravind, H. Selvaraj, S. Ferro, M. Sundaram, An integrated (electro- and bio-oxidation) approach for remediation of industrial wastewater containing azo-dyes: understanding the degradation mechanism and toxicity assessment, Journal of Hazardous Materials 318 (2016) 203–215.
[11] P. Zucca, G. Cocco, F. Sollai, E. Sanjust, Fungal laccases as tools for biodegradation of industrial dyes, Biocatalysis 1 (2015) 82–108.
[12] H. Fu, X.-X. Song, L. Wu, C. Zhao, P. Wang, C.-C. Wang, Room-temperature preparation of MIL-88A as a heterogeneous photo-Fenton catalyst for degradation of rhodamine B and bisphenol A under visible light, Materials Research Bulletin 125 (2020) 110806.
[13] J. Ma, L. Shi, L. Hou, L. Yao, C. Lu, Z. Geng, Fabrication of graphene/$Bi_{12}O_{17}Cl_2$ as an effective visible-light photocatalyst, Materials Research Bulletin 122 (2020) 110690.
[14] Q. Zhang, J. Zhou, Q. Dai, Y. Yan, B. Yao, C.C. Ng, F. Han, M. Ma, P. Cheah, G. Proctor, Enhanced visible-light photocatalytic activity of one dimensional In_2O_3/In_2TiO_5 nanobelts, Materials Research Bulletin 113 (2019) 102–108.
[15] J. Kundu, B.K. Satpathy, D. Pradhan, Composition[HYPHEN]Controlled CdS/ZnS Heterostructure Nanocomposites for Efficient Visible Light Photocatalytic Hydrogen Generation, Industrial & Engineering Chemistry Research 58 (51) (2019) 22709–22717.
[16] Y. Yu, J. Zhang, X. Wu, W. Zhao, B. Zhang, Nanoporous Single-Crystal-Like $Cd_xZn_{1-x}S$ Nanosheets Fabricated by the Cation-Exchange Reaction of Inorganic-Organic Hybrid ZnS-Amine with Cadmium Ions, Angewandte Chemie International Edition 51 (2012) 897–900.
[17] H. Abid, G. Rekhila, F.A. Ihaddadene, Y. Bessekhouad, M. Trari, Hydrogen evolution under visible light illumination on the solid solution $Cd_xZn_{1-x}S$ prepared by ultrasound-assisted route, International Journal of Hydrogen Energy 44 (2019) 10301–10308.
[18] H. Yin, X. Liu, 0D/2D P-doped $Zn_xCd_{1-x}S$/g-C_3N_4 Heterojunctions towards Highly Efficient Photocatalytic Hydrogen Evolution, Proceedings of Engineering and Technology Innovation 13 (2019) 32–40.
[19] J. Qiu, M. Li, Y. Wan, S. Zhang, H. Wang, J. Yao, One-pot fabrication of $Cd_xZn_{1-x}S$/ZnO nanohybrid using mixed sulfur sources for photocatalysis, Materials Research Bulletin 125 (2020) 110776.
[20] J. Theerthagiri, R. Senthil, J. Madhavan, Synthesis, characterization and optical properties of $Cd_xZn_{1-x}S$ nanocrystals, in: Materials Science Forum, Trans Tech Publications Ltd (2015) 158–167.
[21] H. Zhao, X. Ding, B. Zhang, Y. Li, C. Wang, Enhanced photocatalytic hydrogen evolution along with byproducts suppressing over Z-scheme $Cd_xZn_{1-x}S$/Au/g-C_3N_4 photocatalysts under visible light, Science Bulletin 62 (2017) 602–609.
[22] X. Yan, Z. Jin, Y. Zhang, Y. Zhang, H. Yuan, Sustainable and efficient hydrogen evolution over a noble metal-free WP double modified ZnxCd1 − xS photocatalyst driven by visible-light, Dalton Transactions 48 (29) (2019) 11122–11135.
[23] S. Horoz, O. Baytar, O. Sahin, H. Kilicvuran, Photocatalytic degradation of methylene blue with Co alloyed CdZnS nanoparticles, Journal of Materials Science: Materials in Electronics 29 (2018) 1004–1010.
[24] M. Huang, J. Yu, C. Deng, Y. Huang, M. Fan, B. Li, Z. Tong, F. Zhang, L. Dong, 3D nanospherical $Cd_xZn_{1-x}S$/reduced graphene oxide composites with superior

photocatalytic activity and photocorrosion resistance, Applied Surface Science 365 (2016) 227–239.
[25] J. Wang, B. Li, J. Chen, N. Li, J. Zheng, J. Zhao, Z. Zhu, Enhanced photocatalytic H_2-production activity of $Cd_xZn_{1-x}S$ nanocrystals by surface loading MS (M = Ni, Co, Cu) species, Applied Surface Science 259 (2012) 118–123.
[26] X. Lin, G. Gao, L. Zheng, Y. Chi, G. Chen, Encapsulation of strongly fluorescent carbon quantum dots in metal-organic frameworks for enhancing chemical sensing, Analytical Chemistry 86 (2013) 1223–1228.
[27] H. Li, L. Li, R.-B. Lin, W. Zhou, S. Xiang, B. Chen, Z. Zhang, Porous metal-organic frameworks for gas storage and separation: Status and challenges, EnergyChem 1 (1) (2019) 100006.
[28] I.A. Lazaro, R.S. Forgan, Application of zirconium MOFs in drug delivery and biomedicine, Coordination Chemistry Reviews 380 (2019) 230–259.
[29] M. Li, Y. Liu, C. Shen, F. Li, C.-C. Wang, M. Huang, B. Yang, Z. Wang, J. Yang, W. Sand, One-step Sb(III) decontamination using a bifunctional photoelectrochemical filter, Journal of Hazardous Materials 389 (2020) 121840.
[30] D. Sun, W. Liu, M. Qiu, Y. Zhang, Z. Li, Introduction of a mediator for enhancing photocatalytic performance via post-synthetic metal exchange in metal-organic frameworks (MOFs), Chemical Communications 51 (2015) 2056–2059.
[31] D.-D. Chen, X.-H. Yi, C. Zhao, H. Fu, P. Wang, C.-C. Wang, Polyaniline modified MIL-100(Fe) for enhanced photocatalytic Cr(VI) reduction and tetracycline degradation under white light, Chemosphere 245 (2020) 125659.
[32] X.-H. Yi, S.-Q. Ma, X.-D. Du, C. Zhao, H. Fu, P. Wang, C.-C. Wang, The facile fabrication of 2D/3D Z-scheme g-C_3N_4/UiO-66 heterojunction with enhanced photocatalytic Cr(VI) reduction performance under white light, Chemical Engineering Journal 375 (2019) 121944.
[33] E. Akbarzadeh, H.Z. Soheili, M. Hosseinifard, M.R. Gholami, Preparation and characterization of novel Ag_3VO_4/Cu-MOF/rGO heterojunction for photocatalytic degradation of organic pollutants, Materials Research Bulletin 121 (2020) 110621.
[34] L. Chen, R. Luque, Y. Li, Controllable design of tunable nanostructures inside metal-organic frameworks, Chemical Society Reviews 46 (2017) 4614–4630.
[35] Y. Liu, Y. Wang, H. Wang, P. Zhao, H. Hou, L. Guo, Acetylene black enhancing the electrochemical performance of NiCo-MOF nanosheets for supercapacitor electrodes, Applied Surface Science 492 (2019) 455–463.
[36] C.-C. Wang, X. Wang, W. Liu, The synthesis strategies and photocatalytic performances of TiO_2/MOFs composites: A state-of-the-art review, Chemical Engineering Journal (2020), https://doi.org/10.1016/S1385-8947(19)33016-5.
[37] C.-C. Wang, X.-H. Yi, P. Wang, Powerful combination of MOFs and C_3N_4 for enhanced photocatalytic performance, Applied Catalysis B: Environmental 247 (2019) 24–48.
[38] F. Mu, S. Zhou, Y. Wang, J. Wang, Y. Kong, Bimetallic metal-organic frameworks-derived mesoporous $Cd_xZn_{1-x}S$ polyhedrons for enhanced photocatalytic hydrogen evolution, Journal of Materials Research 34 (2019) 1773–1784.
[39] M. Sun, Q.Q. Wang, C. Qin, C.Y. Sun, X.L. Wang, Z.M. Su, An Amine-Functionalized Zirconium Metal-Organic Polyhedron Photocatalyst with High Visible-Light Activity for Hydrogen Production, Chemistry-A European Journal 25 (2019) 2824–2830.
[40] J. Qiu, X.F. Zhang, X. Zhang, Y. Feng, Y. Li, L. Yang, H. Lu, J. Yao, Constructing $Cd_{0.5}Zn_{0.5}S$@ZIF-8 nanocomposites through self-assembly strategy to enhance Cr (VI) photocatalytic reduction, Journal of Hazardous Materials 349 (2018) 234–241.
[41] F.-X. Wang, X.-H. Yi, C.-C. Wang, J.-G. Deng, Photocatalytic Cr(VI) reduction and organic-pollutant degradation in a stable 2D coordination polymer, Chinese Journal of Catalysis 38 (2017) 2141–2149.
[42] X.H. Yi, F.X. Wang, X.D. Du, P. Wang, C.C. Wang, Facile fabrication of BUC-21/g-C_3N_4 composites and their enhanced photocatalytic Cr(VI) reduction performances under simulated sunlight, Applied Organometallic Chemistry 33 (2019) e4621.
[43] C. Zhao, Z. Wang, X. Li, X. Yi, H. Chu, X. Chen, C.-C. Wang, Facile fabrication of BUC-21/$Bi_{24}O_{31}Br_{10}$ composites for enhanced photocatalytic Cr(VI) reduction under white light, Chemical Engineering Journal 389 (2020) 123431.
[44] X. Wang, Y.-X. Li, X.-H. Yi, C. Zhao, P. Wang, J. Deng, C.-C. Wang, Photocatalytic Cr (VI) elimination over BUC-21/N-$K_2Ti_4O_9$ Composites: Big Difference in Performances Resulting from Small Difference in Composition, Chinese Journal of Catalysis (2020), https://doi.org/10.1016/S1872-2067(20)63629-4.
[45] X. Wang, W. Liu, H. Fu, X.H. Yi, P. Wang, C. Zhao, C.C. Wang, W. Zheng, Simultaneous Cr(VI) reduction and Cr(III) removal of bifunctional MOF/Titanate nanotube composites, Environmental Pollution 249 (2019) 502–511.
[46] B. Jiang, Y. Gong, J. Gao, T. Sun, Y. Liu, N. Oturan, M.A. Oturan, The reduction of Cr(VI) to Cr(III) mediated by environmentally relevant carboxylic acids: State-of-the-art and perspectives, Journal of Hazardous Materials 365 (2019) 205–226.
[47] J. Xiang, H. Wang, X. Wang, X. Chen, T. Wu, H. Wan, Y. Liu, H. Wang, Colloidal $Cd_xZn_{1-x}S$ nanocrystals as efficient photocatalysts for H_2 production under visible-light irradiation, RSC Advances 9 (2019) 4001–4007.
[48] Q. Liang, J. Jin, C. Liu, S. Xu, C. Yao, Z. Li, Fabrication of the ternary heterojunction $Cd_{0.5}Zn_{0.5}S$@UiO-66@g-C_3N_4 for enhanced visible-light photocatalytic hydrogen evolution and degradation of organic pollutants, Inorganic Chemistry Frontiers 5 (2018) 335–343.
[49] L. Hu, H. Hu, W. Lu, Y. Lu, S. Wang, Novel composite $BiFeO_3/ZrO_2$ and its high photocatalytic performance under white LED visible-light irradiation, Materials Research Bulletin 120 (2019) 110605.
[50] K. Shu, F. Chen, W. Shi, F. Guo, Y. Tang, H. Ren, M. Li, Construction of $DyVO_4$/nitrogen deficient g-C_3N_4 composite for enhanced visible-light photocatalytic activity for tetracycline degradation, Materials Research Bulletin 124 (2020) 110766.
[51] S. Tian, S. Xu, J. Liu, C. He, Y. Xiong, P. Feng, Highly efficient removal of both cationic and anionic dyes from wastewater with a water-stable and eco-friendly Fe-MOF via host-guest encapsulation, Journal of Cleaner Production 239 (2019) 117767.
[52] M. Sakar, T.O. Do, Metal–Organic Frameworks for Photocatalytic Environmental Remediation, Photocatalytic Functional Materials for Environmental Remediation (2019) 309–341.
[53] Q. Xiang, J. Yu, P.K. Wong, Quantitative characterization of hydroxyl radicals produced by various photocatalysts, Journal of Colloid and Interface Science 357 (2011) 163–167.
[54] L.A. Alfonso-Herrera, A.M. Huerta-Flores, L.M.T. Martínez, D.J. Ramírez-Herrera, J. Rivera-Villanueva, M-008: A stable and reusable metalorganic framework with high crystallinity applied in the photocatalytic hydrogen evolution and the degradation of methyl orange, Journal of Photochemistry and Photobiology A: Chemistry 389 (2020) 112240.
[55] M. Li, J. Li, Z. Jin, 0D/2D spatial structure of $Cd_xZn_{1-x}S$/Ni-MOF-74 for efficient photocatalytic hydrogen evolution, Dalton Transactions (2020), https://doi.org/10.1039/D0DT00271B.
[56] Q. Yang, Q. Xu, H.L. Jiang, Metal-organic frameworks meet metal nanoparticles: synergistic effect for enhanced catalysis, Chemical Society Reviews 46 (2017) 4774–4808.
[57] J.-C. Wang, J. Ren, H.-C. Yao, L. Zhang, J.-S. Wang, S.-Q. Zang, L.-F. Han, Z.-J. Li, Synergistic photocatalysis of Cr(VI) reduction and 4-Chlorophenol degradation over hydroxylated α-Fe_2O_3 under visible light irradiation, Journal of Hazardous Materials 311 (2016) 11–19.
[58] X. [58] Hu, H. Ji, F. Chang, Y. Luo, Simultaneous photocatalytic Cr(VI) reduction and 2, 4, 6-TCP oxidation over g-C_3N_4 under visible light irradiation, Catalysis Today 224 (2014) 34–40.
[59] L. Shi, T. Wang, H. Zhang, K. Chang, X. Meng, H. Liu, J. Ye, An amine-functionalized iron(III) metal-organic framework as efficient visible-light photocatalyst for Cr (VI) reduction, Advanced Science 2 (2015) 1500006.
[60] O. Carp, C.L. Huisman, A. Reller, Photoinduced reactivity of titanium dioxide, Progress in Solid State Chemistry 32 (2004) 33–177.